Spatial-Attraction-Based Markov Random Field Approach for Classification of High Spatial Resolution Multispectral Imagery

Hua Zhang, Wenzhong Shi, Yunjia Wang, Ming Hao, and Zelang Miao

***Abstract*—This letter presents a novel spatial-attraction-based Markov random field (MRF) (SAMRF) approach for high spatial resolution multispectral imagery (HSRMI) classification. First, the initial class label and class membership for each pixel are obtained by applying the maximum likelihood classifier (MLC) classification for the HSRMI. Second, to reduce the oversmooth classification in the traditional MRF, an adaptive weight MRF model is introduced by integrating the spatial attraction model into the traditional MRF. Finally, the initial classification map, generated in the first step, will be refined though the SAMRF regularization. Two different experiments were performed to evaluate the performance of the SAMRF, in comparison with standard MLC and MRF. Experimental results indicate that the SAMRF method achieved the highest accuracy, hence, providing an effective spectral–spatial classification method for the HSRMI.**

***Index Terms*—Classification, high spatial resolution multispectral imagery (HSRMI), Markov random field (MRF), spatial attraction.**

I. Introduction

IMAGE classification plays an important role in remote sensing applications. With the available high spatial resolution multispectral imagery (HSRMI) such as IKONOS, QuickBird, SPOT-5, etc., more detailed ground information containing abundant spectral and spatial characteristics can be obtained for image classification, while the increase in the spatial resolution always leads to increased spectral similar and complex spatial arrangement. The conventional pixelwise classification methods, including support vector machines, maximum likelihood classifier (MLC), etc., only utilize spectral information regardless of spatial information such as texture and context; consequently, they are inadequate for HSRMI classification [1]. In addition, HSRMI contains abundant spatial information which can help for accurate interpretation. Thus, in recent years, many spectral–spatial classification methods, which integrate spectral with spatial characteristics, had been proved to be successful in improving the classification [2]–[6].

Markov random field (MRF) is widely used to improve the classification accuracy by incorporating spatial contextual information into classification [2], [4], [6]. The MRF is a probabilistic model which extracts spatial contextual information through the dependence among neighboring pixels [7]. Although MRF commonly can obtain better classification result than the pixelwise classifier [4], the spatial weighing coefficients, which determine the neighborhood pixels' contributions to the center pixel, are difficult to acquire [8]. Neighbor pixels' influences on the center pixel are treated equally in the traditional MRF; as a result, the classification accuracy is improved in homogeneous areas, while a lot of errors frequently occur on boundary areas losing significant detailed features and producing large patches [9], [10]. Tso and Olsen [11] introduced multiscale fuzzy lines to MRF for restricting the oversmooth classification and estimated the MRF model parameter based on probability histogram analysis to the edge pixels. Tarabalka *et al.* [2] integrated the fuzzy no edge/edge function into the spatial energy function to preserve the edge pixels. Zhang *et al.* [12] introduced a relative homogeneity index (RHI) to obtain the suitable spatial weight. However, these edge detection and RHI calculation algorithms are always sensitive to noise existing in the image. In addition, the spatial weights were determined according to distances between neighbor pixels and center pixel [4], [13], while only the distance is taken into account regardless of the local image statistics in these approaches. A more efficient method is required to cope with such boundary pixels and spatial weight estimation issues.

This letter presents a novel spatial-attraction-based MRF (SAMRF) approach for the spectral–spatial classification of HSRMI. The spatial attraction is introduced to estimate adaptive weight parameters for MRF model in order to improve the classification performance. The proposed approach was tested through two different experiments. The results demonstrated that the SAMRF approach can achieve improved classification accuracy.

Manuscript received April 24, 2013; revised June 6, 2013; accepted June 13, 2013. Date of publication September 4, 2013; date of current version November 25, 2013. This work was supported in part by the National Natural Science Foundation of China, under Grants 41201451, 41331175, and 51174287, by the Fundamental Research Funds for the Central Universities under Grant 2010QNB13, by the Scientific Research Foundation of Key Laboratory for Land Environment and Disaster Monitoring of SBSM under Grant LEDM2010B11, and by a project funded by the Priority Academic Program Development of Jiangsu Higher Education Institutions.

H. Zhang, Y. Wang, and M. Hao are with the Key Laboratory for Land Environment and Disaster Monitoring of SBSM, China University of Mining and Technology, Xuzhou 221116, China (e-mail: zhhuamesi@gmail.com; wyj4139@163.com; haomingcumt@gmail.com).

W. Shi is with the Department of Land Surveying and Geo-Informatics, The Hong Kong Polytechnic University, Kowloon, Hong Kong (e-mail: lswzshi@polyu.edu.hk).

Z. Miao is with the Key Laboratory for Land Environment and Disaster Monitoring of SBSM, China University of Mining and Technology, Xuzhou 221116, China, and also with the Department of Land Surveying and Geo-Informatics, The Hong Kong Polytechnic University, Kowloon, Hong Kong (e-mail: cumtzlmiao@gmail.com).

Color versions of one or more of the figures in this paper are available online at http://ieeexplore.ieee.org.

Digital Object Identifier 10.1109/LGRS.2013.2268968

II. SAMRF Classification Scheme

In this section, we first describe the traditional MRF model. Then, the improved MRF model-based spatial attraction is presented. Last, the proposed approach's procedure is provided.

A. Classification Based on MRF

Suppose that a $\mathbf{d}$-band remotely sensed image is given, which can be considered as a set of N pixel vectors $X = \{x_1, x_2, \ldots, x_N\} \subset R^d$. $c = \{c_1, c_2, \ldots, c_k, \ldots, c_K\}$ denotes the class label of image, where $k = 1, \ldots, K$, and K is the number of classes. The maximum *a posteriori* is applied to acquire the labels of pixels; for pixel x, the formulation is described as

$$c^* = \arg\max \{p(x|c)p(c)\} \tag{1}$$

where $p(x|c)$ is the conditional probability distribution in the Gaussian distribution model and $p(c)$ is *a priori* probability distribution of the label layer. Its spectral energy function can be represented as (2) for pixel x_i

$$u_{\text{spectral}}(x_i, c_k) = \frac{1}{2}\ln\left|2\pi\sum_k\right| + \frac{1}{2}(x_i - u_k)^T\sum_k^{-1}(x_i - u_k) \tag{2}$$

where u_k and $\sum_k$ are the mean vector and covariance matrix of class k, respectively; they can be calculated based on the training samples. According to the Hammersley–Clifford theorem and the Gibbs theorem [14], *a priori* probability $p(c)$ can be represented as

$$p(c) = \frac{1}{Z}\exp\{-u(c)\}. \tag{3}$$

The spatial energy of pixel x_i can be written as

$$u_{\text{spatial}}(c(x_i)) = \beta\sum_{j\in N_i} I(c(x_i)), c(x_j)) \tag{4}$$

$$I(c(x_i), c(x_j)) = \begin{cases} -1 & c(x_i) = c(x_j) \\ 0 & c(x_i) \neq c(x_j) \end{cases} \tag{5}$$

where Z is the normalizing constant, $u(c)$ is the energy function, $N = \{N_i, i \in S\}$ describes the spatial relationships of pixels in the label layer of the MRF model, N_i denotes the neighbors of pixel x_i, $i \notin N_i$, $c(x_i)$ denotes the class label of pixel x_i, and $c(x_j)$ is the neighbor class label of pixel x_i, $j \in N_i$. Formula (5) is the Potts model in MRF and used to describe the class label *a priori* probability, and β is a penalty coefficient which is used to control the strength between pixel x_i and its neighbor pixel $j \in N_i$ and is commonly determined by experience. Therefore, (1) can be solved by

$$U(x_i, c(x_i)) = \arg\min\left(u_{\text{spectral}}(x_i, c_k) + u_{\text{spatial}}(c(x_i))\right). \tag{6}$$

B. SAMRF Classification

As can be seen from (5), the neighbor pixels have the equal influences on the center pixel x_i regardless of the distances between neighbor and center pixels, the local image statistics, and whether the neighbor pixel is a boundary pixel or not. However, according to the first law of geography, there exist spatial autocorrelations in the pixels in image, that is to say, close pixels more likely belong to the same classes than pixels far apart. The MRF model is based on the first law of geography. Thus, the traditional MRF model is isotropic and not suitable in practice. Furthermore, ignoring the boundary pixels will result in overcorrection [3]. As we know, in the law of universal gravitation, spatial attractions exist in objects, and the value of spatial attraction is determined by the distance and quality of objects; the law of universal gravitation exactly describes spatial attractions between objects. Thus, we can use the law of universal gravitation model to describe the weights between center pixel and neighbor pixels. Therefore, in this letter, the SAMRF model based on traditional MRF is proposed to obtain suitable weight coefficient for improving the classification performance.

$N_{i,0}$	$N_{i,1}$	$N_{i,2}$
$N_{i,3}$	i	$N_{i,4}$
$N_{i,5}$	$N_{i,6}$	$N_{i,7}$

(a)

$1/\sqrt{2}$	1	$1/\sqrt{2}$
1	i	1
$1/\sqrt{2}$	1	$1/\sqrt{2}$

(b)

Fig. 1. Pixel spatial attraction at the neighbors of pixel i at 3×3 window. (a) Neighbor of pixel i. (b) Distances between pixel i and its neighbors.

In the SAMRF model, (5) is represented as (7), and (4) becomes (8)

$$I_{\text{SA}}(c(x_i), c(x_j)) = \begin{cases} -w_{ij} & c(x_i) = c(x_j) \\ 0 & c(x_i) \neq c(x_j) \end{cases} \tag{7}$$

$$u_{\text{spatial-sa}}(c(x_i)) = \beta\sum_{j\in N_i} I_{\text{SA}}(c(x_i)), c(x_j)) \tag{8}$$

where w_{ij} is the spatial attraction between the neighbor pixel j and center pixel i and can be used to describe the weights between center pixel and neighbor pixels. How to calculate w_{ij} becomes important in the SAMRF. The proposed method is performed at 3×3 window [see Fig. 1(a)]; the rationale of this letter goes as follows.

1) The spatial attractions only exist at the 3×3 window [see Fig. 1(a)].
2) The spatial attractions are neglected outside of the 3×3 window.
3) The spatial attractions only exist between the same class subpixels contained in the center pixel and in the neighbor pixel.

In the SAMRF model, the class label and the posterior probability (classification membership) output of the classification had been obtained by the MLC. Each pixel is represented as a posterior probability vector which denotes fractions of every class in one pixel. Therefore, the spatial attractions, between the center pixel and the neighbor pixel at the subpixel scale, can be represented as

$$w_{ij} = z(p_i) * z(p_j) * \frac{1}{R_{i,j}^2} \tag{9}$$

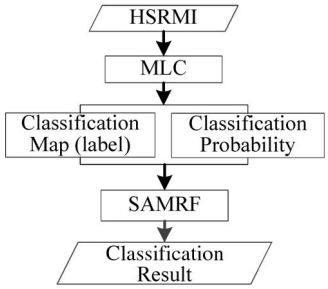

Fig. 2. Flowchart of the proposed SAMRF classification procedure.

where i denotes the center pixel i, $j \in N_{i,j}\{j = 0, 1, 2, \ldots, 7\}$ denotes the neighbor pixels of pixel i, z is the class label of the center pixel i, p_i is the fraction value of class z in pixel i, and p_j is the fraction value of class z in pixel j. $R_{i,j}$ is the distance between pixel i and pixel j; Fig. 1(b) shows the distance $R_{i,j}$ between pixel i and its neighbors at 3×3 window.

Therefore, (1) can be solved by

$$U\left(x_i, c(x_i)\right) = \arg\min\left(u_{\text{spectral}}(x_i, c_k) + u_{\text{spatial-sa}}\left(c(x_i)\right)\right). \tag{10}$$

To solve (10), many algorithms can be adopted, such as iteration condition model (ICM), simulated annealing, and maximum *a posteriori* margin [14], due to the computational complexity; in this letter, (10) is solved by the ICM method, and the initial label of the image is obtained by the MLC method.

The contributions of SAMRF are as follows: 1) Distances between the center pixel and neighbor pixels are taken into account, and 2) the class fractions (classification membership) in a pixel are used in spatial attraction model to better describe the different influences on the center pixel from the neighbor pixels. Thus, the proportion of spatial term for the boundary pixel may be controlled by the adaptive weights (spatial attractions). To a certain extent, the SAMRF can solve the boundary pixel classification errors which are at the risk of oversmooth, losing significant details.

The flowchart of the SAMRF classification method is shown in Fig. 2. Given a high spatial resolution multispectral image, the image is first classified based on MLC; then, the class label and the posterior probability for each pixel are estimated, respectively. Second, the spatial attractions between the center pixels and its neighbor pixels are calculated for determining the different influences based on the spatial attraction formulation using the acquired class label and posterior probability for each pixel. Finally, the SAMRF is resolved by the ICM algorithm to obtain the improved classification.

The implementation of the SAMRF classification method includes the following three steps.

Step 1—Classification by MLC Method: Based on the remotely sensed data and ground true data, enough training samples are selected using the stratified random sampling method. Then, the classification is performed using MLC method to output posterior probability (or class membership) $p(c|x)$ of each pixel. Last, based on the Bayes' theory, pixel x is assigned as class c if $P(c|x) = \max_{1 \le r \le k} P(r|x)$. The class label and posterior probability for each pixel are recorded for the steps of SAMRF classification.

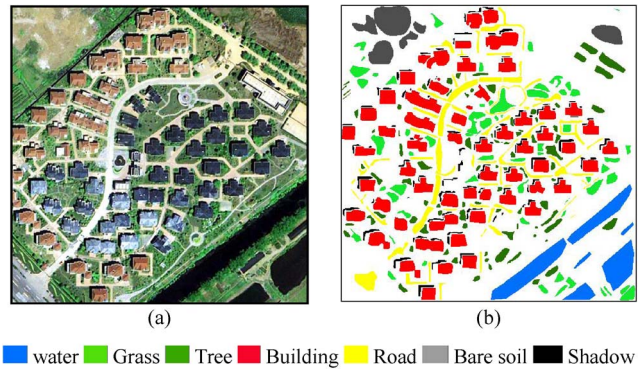

Fig. 3. (a) QuickBird image of the suburb of Xuzhou. (b) Reference data.

Step 2—Computation of Spatial Attraction: Based on the class label and posterior probability for each pixel acquired in *Step 1*, the spatial attractions for each pixel are calculated and recorded according to (9) for the steps of the SAMRF classification.

Step 3—Classification Based on SAMRF: Formula (2) is used to calculate the spectral energy for each pixel. Then, the spatial energy for each pixel is calculated by (8) based on a setting β. Finally, the classification result is obtained through minimizing the energy function by solving (10) using the ICM algorithm.

III. Experimental Results and Discussion

The proposed SAMRF classification algorithms are programmed in Matlab7.8. Two experiments were conducted to test the SAMRF performance. Comparisons were made between SAMRF, equal-weighted MRF (EWMRF), and standard MLC in the experiments. In all experiments, the parameter β for the ICM algorithm is set at 0.6, and the iteration is set at 100. The SAMRF and EWMRF use the same parameters for comparing the performances of the classifications. The classification classes used in the two experiments are water, grass, tree, building, road, bare soil, and shadow. The reference data are obtained through visual interpretation method based on the well-rectified image; the training samples are selected by using the stratified random sampling method based on the reference data, and the left of reference data is treated as the testing samples. The producer's accuracy, overall accuracy, and Kappa coefficient based on the confusion matrix are used to evaluate the classification performances of the three algorithms [15].

A. Experiment 1: QuickBird Image of Xuzhou Suburb Area

In the first experiment, the 0.61-m-resolution QuickBird (512×512 pixels) image contains three multispectral bands [red, green, and blue (RGB)] of the suburb area of Xuzhou, China, which was acquired on August 2005 [Fig. 3(a)]. Fig. 3(b) shows the reference data. Table I describes the training and testing samples of the experiment 1.

Fig. 4(a)–(c) shows the classification results derived from the MLC, EWMRF, and SAMRF, respectively. As shown in Fig. 4(a), because many pixels are mixed pixels, MLC produces a map with "salt and pepper" without considering contextual

TABLE I
NUMBER OF SAMPLES, PRODUCER'S ACCURACY, OVERALL ACCURACY, AND KAPPA COEFFICIENT OF CLASSIFICATION IN EXPERIMENT 1

Class	Number of Training samples	Number of Testing samples	MLC	EWMRF	SAMRF
Water	1039	9348	86.44%	95.03%	95.39%
Grass	998	8973	77.67%	84.00%	89.09%
Tree	838	7537	73.40%	70.72%	75.20%
Building	3166	28486	78.75%	94.24%	95.71%
Road	1185	10599	91.25%	97.22%	95.33%
Bare soil	712	6376	85.40%	91.64%	90.56%
Shadow	443	3988	63.44%	46.19%	84.90%
Overall Accuracy			80.55%	86.51%	91.79%
Kappa Coefficient			0.7592	0.8291	0.8954

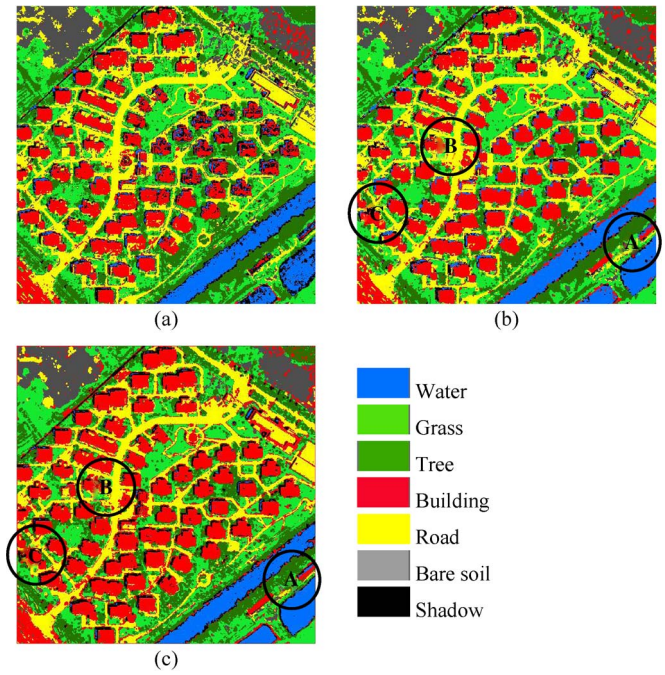

Fig. 4. (a), (b), and (c) are the classification results based on MLC, EWMRF, and SAMRF, respectively.

information. Fig. 4(b) and (c) shows more homogeneous regions than MLC, and many noises are removed. SAMRF gives a more satisfactory classification result than EWMRF, seen from A, B, and C regions in Fig. 4(b) and (c), and SAMRF preserves many detailed features, while oversmooth results occur on boundary areas and produce large patches in EWMRF. The reason is that the SAMRF used the spatial attractions as the adaptive weights for every pixel to control the proportion of spatial terms in MRF. Table I lists the comparisons between producer accuracy, overall classification accuracy, and Kappa coefficient of MLC, EWMRF, and SAMRF. As can be seen from Table I, because the spatial contexture information is considered in EWMRF and SAMRF, EWMRF and SAMRF all yield higher classification accuracies than MLC. The SAMRF gives the best overall accuracy and most of the best class producer's accuracies. According to the results of McNemar's test, the MLC, EWMRF, and SAMRF classification accuracies are statistically significant at the 5% level of significance [16], [17].

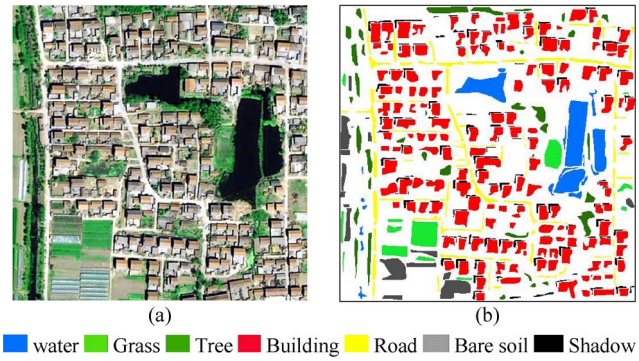

Fig. 5. (a) QuickBird image of the urban center of Xuzhou. (b) Reference data.

TABLE II
NUMBER OF SAMPLES, PRODUCER'S ACCURACY, OVERALL ACCURACY, AND KAPPA COEFFICIENT OF CLASSIFICATION IN EXPERIMENT 2

Class	Number of Training samples	Number of Testing samples	MLC	EWMRF	SAMRF
Water	1007	9047	93.68%	95.94%	96.30%
Grass	523	4711	82.25%	84.91%	85.95%
Tree	678	6098	60.13%	71.30%	79.49%
Building	3923	35306	74.53%	77.71%	82.00%
Road	932	8385	95.40%	94.55%	95.00%
Bare soil	565	5087	95.34%	93.39%	94.85%
Shadow	575	5103	84.58%	98.75%	95.30%
Overall Accuracy			80.68%	84.33%	87.08%
Kappa Coefficient			0.7481	0.7938	0.8281

B. Experiment 2: QuickBird Image of Xuzhou Urban Center Area

In the second experiment, the 0.61-m-resolution QuickBird (512 × 512 pixels) image contains three multispectral bands (RGB) of the urban center area of Xuzhou, China, which was acquired on August 2005 [Fig. 5(a)]. Fig. 5(b) shows the reference data. Table II describes the training and testing samples of the experiment 2.

Fig. 6(a)–(c) shows the classification maps obtained using the MLC, EWMRF, and SAMRF, respectively. As shown in Fig. 6(a), because many pixels are mixed pixels, using spectral information of pixels alone, MLC produces a map with "salt and pepper" without considering contextual information. Fig. 6(b) and (c) shows more homogeneous regions than MLC, and many noises are removed. Compared with EWMRF, SAMRF gives a more satisfactory classification result, seen from A, B, and C regions in Fig. 6(b) and (c); oversmooth results occur on the boundary pixels in the EWMRF classification map, while SAMRF can preserve many detailed features. The reason is that the SAMRF used the spatial attractions as the adaptive weights for every pixel to control the proportion of spatial terms in MRF. Table II lists the comparisons between producer accuracy, overall classification accuracy, and Kappa coefficient of MLC, EWMRF, and SAMRF. As seen from Table II, because the spatial contexture information is considered in EWMRF and SAMRF, EWMRF and SAMRF all yield higher classification accuracies than MLC. The SAMRF gives the best overall accuracy and most of the best class producer's accuracies. Following the results of McNemar's test, the MLC,

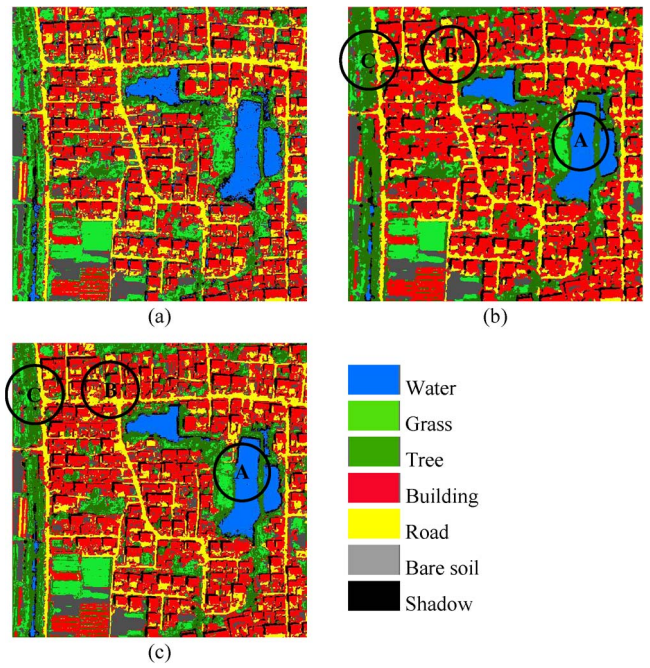

Fig. 6. (a), (b), and (c) are the classification results based on MLC, EWMRF, and SAMRF, respectively.

EWMRF, and SAMRF classification accuracies are statistically significant at the 5% level of significance.

From Table I and Table II, we can see that the tree class had the lowest classification performance. The reason may be that the trees are always in scattered distribution and have the similar spectral feature with the grass; consequently, they are frequently misclassified as other classes. However, in the SAMRF, the tree classification accuracies are improved highly, which convinces that the SAMRF can preserve the detailed features to a certain extent.

Above all, the proposed SAMRF with adaptive weights from neighbor pixel outperforms the EWMRF with equal weights and MLC in terms of overall classification accuracy and Kappa coefficient. Experimental results indicate that the SAMRF approach is competitive and often performs more accurately than the EWMRF and standard MLC approaches.

IV. Conclusion

A novel SAMRF approach for the spectral–spatial classification of HSRMI has been presented in this letter. First, the class label and class membership of each pixel are generated by classification using MLC method based on the HSRMI. Second, adaptive weight MRF is introduced to provide spatial contexture information. In the adaptive weights, the spatial attractions between center pixel and its neighbor pixels are calculated to determine contributions to the center pixel from the neighbor pixels considering the distances and image statistics. The SAMRF contributes that the appropriate weighs for MRF model can be obtained and the risk of oversmooth for boundary pixels can be reduced to a certain extent. Finally, the final classification map is obtained through the MRF regularization. Two experiments were carried out to evaluate the performance of the SAMRF. Compared with the standard MLC and EWMRF, the SAMRF achieves enhancements in both the classification accuracy and visual interpretation. These evince that the SAMRF is an effective classifier for HSRMI.

In our future work, more work will be carried out on methods of determining the appropriate penalty coefficient β, and the SAMRF will be applied for other types of remotely sensed images, etc.

References

[1] D. A. Landgrebe, *Signal Theory Methods in Multispectral Remote Sensing*. New York, NY, USA: Wiley, 2003.

[2] Y. Tarabalka, M. Fauvel, and J. Chanussot, "SVM- and MRF-based method for accurate classification of hyperspectral images," *IEEE Geosci. Remote Sens. Lett.*, vol. 7, no. 4, pp. 736–740, Oct. 2010.

[3] A. K. Shackelford and C. H. Davis, "A hierarchical fuzzy classification approach for high-resolution multispectral data over urban areas," *IEEE Trans. Geosci. Remote Sens.*, vol. 41, no. 9, pp. 1920–1932, Sep. 2003.

[4] Y. D. Zhao, L. P. Zhang, and P. X. Li, "Classification of high spatial resolution imagery using improved Gaussian Markov random-field-based texture features," *IEEE Trans. Geosci. Remote Sens.*, vol. 45, no. 5, pp. 1458–1468, May 2007.

[5] M. Pesaresi and J. A. Benediktsson, "A new approach for the morphological segmentation of high-resolution satellite imagery," *IEEE Trans. Geosci. Remote Sens.*, vol. 39, no. 2, pp. 309–320, Feb. 2001.

[6] A. Farag, R. Mohamed, and A. El-Baz, "A unified framework for map estimation in remote sensing image segmentation," *IEEE Trans. Geosci. Remote Sens.*, vol. 43, no. 7, pp. 1617–1634, Jul. 2005.

[7] S. Z. Li, *Markov Random Field Modeling in Image Analysis*. New York, NY, USA: Springer-Verlag, 2010.

[8] B. Tso and P. M. Mather, "Classification of multisource remote sensing imagery using a genetic algorithm and Markov random fields," *IEEE Trans. Geosci. Remote Sens.*, vol. 37, no. 3, pp. 1255–1260, May 1999.

[9] X. Jia and J. A. Richards, "Managing the spectral–spatial mix in context classification using Markov random fields," *IEEE Geosci. Remote Sens. Lett.*, vol. 5, no. 2, pp. 311–314, Apr. 2008.

[10] X. Wang and H. Wang, "Markov random field modeled range image segmentation," *Pattern Recognit. Lett.*, vol. 25, no. 3, pp. 367–375, Feb. 2004.

[11] B. Tso and R. C. Olsen, "A contextual classification scheme based on MRF model with improved parameter estimation and multiscale fuzzy line process," *Remote Sens. Environ.*, vol. 97, no. 1, pp. 127–136, Jul. 2005.

[12] B. Zhang, S. S. Li, X. P. Jia, L. R. Gao, and M. Peng, "Adaptive Markov random field approach for classification of hyperspectral imagery," *IEEE Geosci. Remote Sens. Lett.*, vol. 8, no. 5, pp. 973–977, Sep. 2011.

[13] Q. Zhang, L. P. Zhang, and X. Huang, "Classification of high-spatial resolution imagery based on distance-weighted Markov random field with an improved iterative conditional mode method," *Int. J. Remote Sens.*, vol. 32, no. 24, pp. 9843–9868, Dec. 2010.

[14] A. H. S. Solberg, T. Taxt, and A. K. Jain, "A Markov random field model for classification of multisource satellite imagery," *IEEE Trans. Geosci. Remote Sens.*, vol. 34, no. 1, pp. 100–113, Jan. 1996.

[15] R. G. Congalton, R. G. Oderwald, and R. A. Mead, "Assessing Landsat classification accuracy using discrete multivariate statistical techniques," *Photogramm. Eng. Remote Sens.*, vol. 49, no. 12, pp. 1671–1678, Dec. 1983.

[16] G. M. Foody, "Thematic map comparison evaluating the statistical significance of differences in classification accuracy," *Photogramm. Eng. Remote Sens.*, vol. 70, no. 5, pp. 627–633, May 2004.

[17] D. P. McKenzie, A. J. Mackinnon, N. Peladeau, P. Onghena, P. C. Bruce, D. M. Clarke, S. Haarrigan, and P. D. McGorry, "Comparing correlated Kappas by Resampling: Is one level of agreement significantly different from another?" *J. Psychiatr. Res.*, vol. 30, no. 6, pp. 483–492, Nov./Dec. 1996.